PAPER

Capillary instability on an elastic helix

Sunghwan Jung,[a] Christophe Clanet[b] and John W. M. Bush[*c]

We present the results of a combined experimental and theoretical investigation of the capillary instability of an elastic helical thread bound within a fluid. The influence of the thread's elastic energy on the classic Rayleigh–Plateau instability is elucidated. The most unstable wavelength can be substantially increased by the influence of the helical coil. The relation between our system and the capture thread of the orb-spider is discussed.

1 Introduction

Capillary forces dominate gravity for fluid systems small relative to the millimetric capillary length, and so play a critical role in the lives of insects and spiders.[1,2] Surface energy may also interact with flexible bodies through inducing elastic deformation energies associated with either stretching, bending, or twisting. Specifically, flexible sheets may be folded into complex 3D structures solely through the action of capillary forces. Such self-assembly is termed "capillary origami".[3–5] Natural examples of capillary origami have been examined in the context of floating flowers[6,7] and arise on the wing of the butterfly[8] and the leg of the water strider.[9]

The coupling between capillarity and elastic energy can be characterized by the elastocapillary number; N_{EC}, the ratio of elastic to surface energy. As shown in Fig. 1, examples of $N_{EC} \gg 1$ include the capillary instability of a thin fluid layer on a rigid fibre.[10] In the regime of $N_{EC} \leq 1$, the solid's shape may be altered by capillary, which may cause it to bend, stretch, or twist. In previous studies of capillary origami,[4] surface tension has coupled with bending energy, so the relevant elastocapillary number is $N_{EC} = B/(\gamma l_B^2)$ where B is the bending stiffness per unit width, l_B the radius of curvature, and γ the surface tension. When an elastic object is twisted, torsion may dominate bending. The torsional energy for a stretchable coil depends on its spring constant κ, and the relevant torsional elastocapillary number is $N_{EC} = \kappa/\gamma$. A natural example of helical threads coupled to capillarity is the web of the orb spider (Fig. 1).[14,15]

We here investigate the manner in which the classic capillary instability of a fluid thread is modified by the presence of an embedded elastic coil; specifically, how the coupling between interfacial and elastic forces impacts the system. In Section 2,

we present the results of an experimental investigation of elastocapillary instability along a wet helical thread. In Section 3, an accompanying theoretical model is developed, appropriate for an inviscid fluid. Our results are summarized in Section 4.

2 Experiments

Our experiment is designed to investigate the coupling between spring-like elastic threads and capillarity. One of the challenges in scaling up the experiments is to produce an elastic helix that is sufficiently flexible to deform under the influence of surface tension. For such an elastic coil, a flexible polymer (vinyl-polysiloxane; elite double from Zhermack) was cured into a helical mold with radius $r_e \sim 1.8$ mm and coil diameter $D \sim 0.4$ mm.
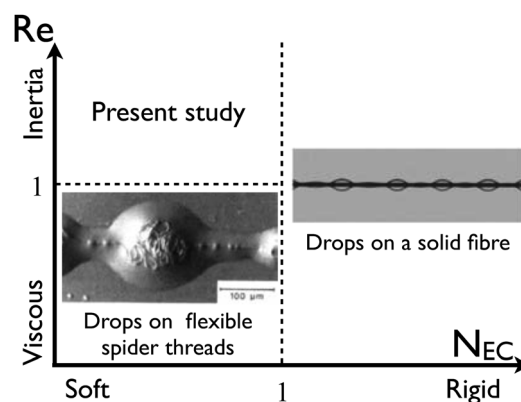

Fig. 1 Elastocapillary coupling on a flexible thread. We delineate regimes according to the Reynolds number, Re = $\rho V r/\eta$, and the elastocapillary number, $N_{EC} = \kappa/\gamma$, where V is a characteristic fluid velocity, r the fiber radius, ρ the fluid density, η the fluid viscosity, κ the thread's spring constant, and γ the surface tension. When a solid fiber is stiff ($N_{EC} \gg 1$), capillarity drives the instability of the coating film, forming drops on the fiber[10] (image from ref. 11). When $N_{EC} \ll 1$ and Re $\ll 1$, the thread may deform in response to the capillary forces, as arises on the capture thread of the orb-web spider (image from ref. 12). Our present study will focus on the regime of high Re and low N_{EC}.

[a]Department of Engineering Science and Mechanics, Virginia Tech, Blacksburg, VA 24061, USA

[b]Laboratoire d'Hydrodynamique (LadHyx), Ecóle Polytechnique, 91128 Palaiseau, France

[c]Department of Mathematics, Massachusetts Institute of Technology, Cambridge, MA 02139, USA. E-mail: bush@math.mit.edu

A schematic illustration of our experimental set-up is presented in Fig. 2(a). The ends of the coil are held and pre-stretched to a length L by two arms connected to a linear stage. The spacing between coils ζ_e and the spring constant κ vary with this prestretching length L. The dependence of spring constant κ on ζ_e is illustrated in Fig. 2(b). One of three configurations was used to wet the coil, either water in air ($\eta \sim 1$ cSt and $\gamma \sim 70$ dynes cm^{-1}), silicon oil in air ($\eta \sim 5$ cSt and $\gamma \sim 20$ dynes cm^{-1}), or silicon oil in water($\eta \sim 5$ cSt and $\gamma \sim 24$ dynes cm^{-1}). The contact angle of water on the elastic polymer was measured to be approximately $55°$. The elastic coil is supported on an enclosed horizontal rod (diameter 0.3 mm) in order to eliminate its sagging under the influence of gravity. Using the linear stage, the support rod is lifted upward as indicated in Fig. 2(a). The

mean radius of the initial fluid column r_0 is inferred by measuring the difference of the bath volume before and after coil extraction, and is typically $r_0 \sim 1.0$ mm.

The experiments have been performed for low Weber (We = $\rho V^2 r_e/\gamma$) and capillary (Ca = $\eta V/\gamma$) numbers where V is the withdrawal velocity, specifically We $\sim 10^{-3}$ and Ca $\sim 10^{-4}$. Hence, both viscous and inertial effects are negligible relative to surface tension. The Reynolds number is in the intermediate range as Re = We/Ca ~ 10, indicating that the inertial force dominates the viscous force, and so is retained in the stability analysis to be presented in Section 3. The Ohnesorge number (Oh = $\sqrt{\text{We}}/\text{Re}$) ranges from 0.003 to 0.03. Fig. 2(c and d) shows the formation of bounded droplets along an elastic coil. The coil is initially submerged in a fluid bath, then lifted upward by the linear stage at a speed of approximately 1 cm s^{-1} until the fluid-filled coil detaches from the fluid bath. Following detachment, the coil destabilizes and a number of coil-filled drops form along its length. Depending on the prestretched length L, the spacing and the number of drops vary significantly. Fig. 2(c) shows how a coil moderately prestretched to $L = 4.3$ cm becomes unstable. Fig. 2(d) indicates that the analogous instability for a prestretched length $L = 6.9$ cm generates relatively small droplets.

The coil interacts with the fluid column in the manner depicted in Fig. 2. The fluid totally wets the elastic coil without contact lines, so the coil is everywhere coated by fluid. The elastic coils thus lie just beneath the surface, and since they are flexible enough to deform in response to capillary forces, they are axially compressed or stretched. This elastocapillary instability results in a wavelength prescribed by both the surface tension and the spring's initial loading. Fig. 3 shows the dependence of the wavelength of instability on the non-
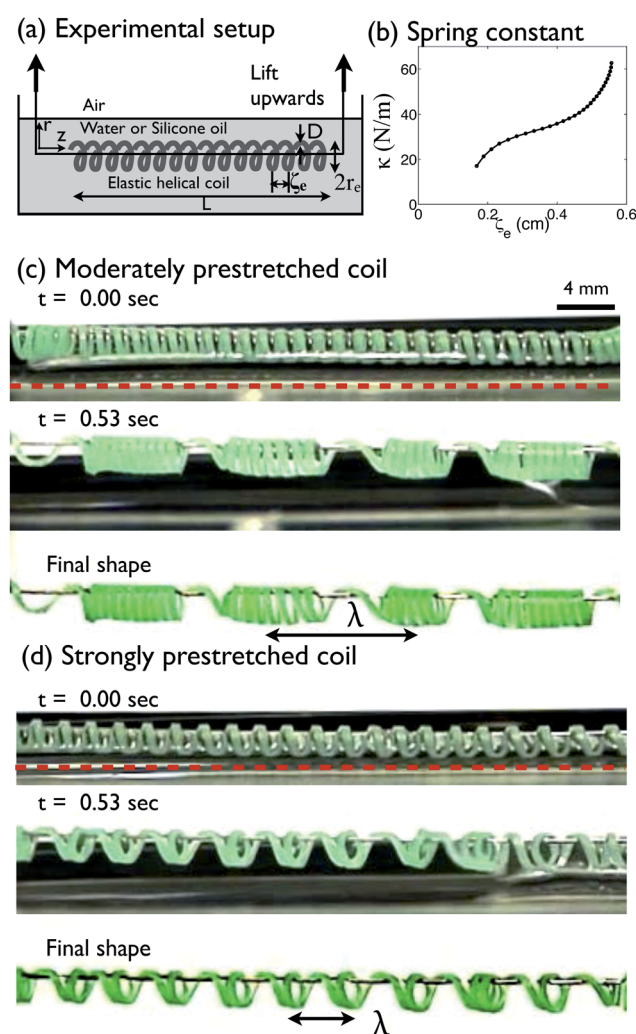

Fig. 2 (a) An elastic coil is suspended on a horizontal wire, submerged into and then withdrawn from a fluid bath, prompting an elastocapillary instability along its length. (b) The dependence of the spring constant κ on the equilibrium coil wavelength ζ_e. (c–d) Image sequences of the elastocapillary instability prompted by coils being withdrawn from a water bath with (c) moderate prestretching ($L = 4.3$ cm), and (d) strong prestretching ($L = 6.9$ cm). In both sequences, the withdrawal speed is approximately 1 cm s^{-1}, and times indicate time since complete withdrawal from the bath.
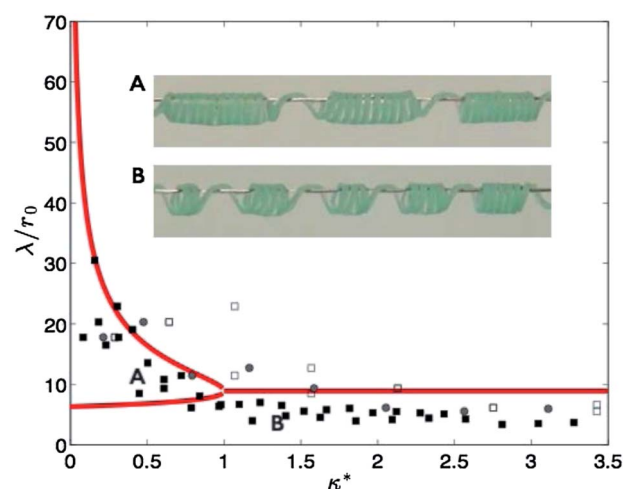

Fig. 3 The dependence of the normalized wavelength of instability λ/r_0 on the nondimensional tension $\kappa^* = \dfrac{\kappa}{\gamma}\dfrac{32}{\pi}\dfrac{\zeta_e r_0^5}{D^4(4\pi^2 r_e^2 + \zeta_e^2)}$. Here, λ is the wavelength of instability and r_0 is the mean radius of the initial fluid column. Experiments with water in air are denoted by closed squares, silicone oil in air by open squares, and silicone oil in water by circles.

dimensional prestretching for coils withdrawn from both oil and water baths.

3 Theoretical modeling

Surface tension acts to minimize surface area. It is thus that a cylindrical jet of water emerging from a kitchen tap pinches off into spherical droplets.[13] In our experiment, as the liquid tries to form drops, it interacts with the elastic coil and the final equilibrium results from the minimization of both surface and elastic energies.

The total energy associated with surface tension, spring tension, and kinetic energy is given by

$$\mathcal{E} = \gamma \iint \mathrm{d}S + \frac{\rho}{2} \iiint |v|^2 \mathrm{d}(\text{vol}) + \frac{\kappa}{2} \int (\zeta - \zeta_\mathrm{e})^2 \frac{\mathrm{d}z}{\zeta}, \qquad (1)$$

where $\mathrm{d}S$ is small area on the interface, $\mathrm{d}(\text{vol})$ a volume element in fluid, ζ the coil spacing and ζ_e its equilibrium value. In the classical analysis of Rayleigh,[13] the energy of the liquid column consists of surface energy and kinetic energy due to fluid motion. In our analysis, we may likewise neglect viscous effects on the basis of the high Reynold numbers. To extend this analysis to include the elastocapillary coupling, the horizontal force balance between the helical spring and ambient hydrodynamic stress must be considered.

The hydrodynamic force acting on the coil in the longitudinal direction at any arbitrary point z^* is determined by the pressure distribution around it. Specifically, the longitudinal force is

$$f_z(z = z^*) = \int_{D_\mathrm{C}} \left(\hat{z} \cdot \tau_{\mathrm{ij}} \cdot \hat{n} \right) \mathrm{d}S \approx \int_{D_\mathrm{C}} p \left(\hat{z} \cdot \hat{n} \right) \mathrm{d}S$$

$$\approx \frac{\partial p}{\partial z} \frac{\pi D^2}{4} = \varepsilon q(kr_0)\sin(kz^*) + \mathcal{O}(\varepsilon^2). \qquad (2)$$

where D_C is the outer surface of the coil, $q(kr_0) = \frac{\pi D^2}{4} \frac{\gamma}{r_0^3} kr_0(1 - (kr_0)^2)$, and r_0 is the mean radius of the initial fluid column. In the last step, the pressure is assumed to be independent of radial position and so prescribed by the boundary shape $R = r_0 - \frac{\varepsilon^2}{(4r_0)} + \varepsilon \cos(kx)$ where ε is the small perturbation on its radius, and volume conservation prescribes the constant term. The Laplace–Young equation thus yields $p = \gamma \left(\frac{1}{R_1} + \frac{1}{R_2} \right) = \frac{\gamma}{r_0} - \varepsilon \frac{\gamma}{r_0^2}(1 - k^2 r_0^2)\cos(kz) + \mathcal{O}(\varepsilon^2)$. The resulting force is balanced by the spring-like force, $\int_0^z \kappa(\zeta - \zeta_\mathrm{e}) \frac{\mathrm{d}z}{\zeta} = \int_0^s f_z \mathrm{d}s \approx \int_0^z \varepsilon q \mathscr{L} \sin(kz) \frac{\mathrm{d}z}{\zeta} + \mathcal{O}(\varepsilon^2)$. Here, we impose the inextensibility of the coil by requiring a constant arc-length ($\mathscr{L} = \sqrt{4\pi^2 r^2 + \zeta^2} = \text{const}$). The spring-like force is now expressed in terms of the coil's stretching from equilibrium as $\kappa(\zeta - \zeta_\mathrm{e}) \sim \varepsilon q \mathscr{L} \sim \sin(kz) + \mathcal{O}(\varepsilon^2)$. The energy associated with the spring-like coil thus becomes

$$\frac{1}{2} \int \kappa(\zeta - \zeta_\mathrm{e})^2 \frac{\mathrm{d}z}{\zeta} \sim \varepsilon^2 \frac{1}{2} \frac{(q\mathscr{L})^2}{\kappa\zeta_\mathrm{e}} \int \sin^2(kz)\mathrm{d}z + \mathcal{O}(\varepsilon^3). \qquad (3)$$

Taking surface tension and kinetic energy into account, the total energy per unit axial length (eqn (1)) then becomes

$$\mathcal{E} = 2\pi\gamma r_0 \left(1 + \frac{\varepsilon^2}{4r_0^2} \left((kr_0)^2 - 1 \right) \right) + \frac{\rho}{2} \pi r_0^2 \frac{I_0(kr_0)}{kr_0 I_1(kr_0)} \left(\frac{\mathrm{d}\varepsilon}{\mathrm{d}t} \right)^2$$

$$+ \frac{2\pi\gamma\varepsilon^2}{r_0\kappa^*}(kr_0)^2 \left(1 - (kr_0)^2 \right)^2 + \mathcal{O}(\varepsilon^3)$$

$$(4)$$

where $\kappa^* \equiv \frac{2\pi}{\gamma} \frac{\kappa\zeta_\mathrm{e}}{(q\mathscr{L})^2} = \frac{\kappa}{\gamma} \frac{32}{\pi} \frac{\zeta_\mathrm{e} r_0^5}{D^4(4\pi^2 r_\mathrm{e}^2 + \zeta_\mathrm{e}^2)}$ denotes the ratio of spring tension to surface tension, I_0 and I_1 are modified Bessel functions of the first kind.

The dispersion relation is obtained from the equilibrium condition ($\delta\mathcal{E}/\delta\varepsilon = 0$). The stability analysis indicates that the fastest growing wavenumber is given by

$$(kr_0)^* = \begin{cases} 1/\sqrt{2} & \text{if} \quad \kappa^* \geq 1 \\ \sqrt{\left(1 \pm \sqrt{1 - \kappa^*} \right)/2} & \text{if} \quad \kappa^* < 1 \end{cases}, \qquad (5)$$

and the associated growth rate is $\sqrt{\rho r_0^3/\gamma}$ ($\sim$15 msec). The result corresponds to the Rayleigh–Plateau instability ($kr_0 = 1/\sqrt{2}$) when $\kappa^* \geq 1$, but bifurcates into two solutions when $\kappa^* < 1$.

In the limit of a stiff spring, $N_\mathrm{EC} \gg 1$, the spring neither compresses nor stretches under the influence of capillarity. The total energy will then consist of two components, surface and kinetic energy, leading to the same solution as the classical Rayleigh–Plateau instability. In the opposite limit ($N_\mathrm{EC} \ll 1$); the spring is so flexible that its coil spacing varies strongly in response to capillarity. Such a strong deformation has a cost in terms of spring energy which is proportional to the square of coil spacing (eqn (3)). However, the surface energy is linearly proportional to the coil spacing, and so negligible relative to the spring energy (eqn (4)). In this limit, the total energy is presumably dominated by spring and kinetic energies and thus has a maximum growth rate at $(kr_0)^* = 0$ or 1.

Fig. 3 shows the comparison of our model results and experimental data. The wavelength of instability λ is roughly independent of κ^* for stiff threads, $\kappa^* > 1$. The trend of longer wavelength for $\kappa^* < 1$ is clearly evident. Theoretically, two stable states exist; one with a shorter and one with a longer wavelength. The longer wavelength is presumably selected in experiments because it is closer to the initial state, which has an infinite wavelength.

4 Conclusion

We have investigated a novel example of elastocapillary instability inspired by the form of spider capture thread.[14,15] Our experiments and accompanying theoretical models indicate that the classical Rayleigh–Plateau instability must be modified through consideration of the coil's elastic energy of deformation.

The elastocapillary coupling examined herein may give insight into the dynamics of spider capture thread[14,15] as well as the instability of soft wire coating in industrial processing.[16] More generally, we expect elastocapillary coupling to arise in a wide range of biological systems.

Acknowledgements

References

1 J. W. M. Bush and D. L. Hu, Walking on water: Biolocomotion at the interface, *Annu. Rev. Fluid Mech.*, 2006, **38**, 339369.

2 J. W. M. Bush, D. L. Hu and M. Prakash, The integument of water-walking arthropods: Form and function, *Adv. Insect Physiol.*, 2008, **34**, 117192.

3 C. Py, P. Reverdy, L. Doppler, J. Bico, B. Roman and C. Baroud, Capillary origami: Spontaneous wrapping of a droplet with an elastic sheet, *Phys. Rev. Lett.*, 2007, **98**, 156103.

4 J. Bico, B. Roman, L. Moulin and A. Boudaoud, Elastocapillary coalescence in wet hair, *Nature*, 2004, **432**, 690.

5 B. Roman and J. Bico, Elasto-capillarity: deforming an elastic structure with a liquid droplet, *J. Phys.: Condens. Matter*, 2010, **22**, 493101.

6 S. Jung, P. M. Reis, J. James, C. Clanet and J. W. M. Bush, Origami in nature, *Phys. Fluids*, 2009, **21**, 91110.

7 P. M. Reis, J. Hure, S. Jung, J. W. M. Bush and C. Clanet, Grabbing water, *Soft Matter*, 2010, **6**, 57055708.

8 Y. Zheng, X. Gao and L. Jiang, Directional adhesion of superhydrophobic butterfly wings, *Soft Matter*, 2007, **3**, 178–182.

9 M. Prakash and J. W. M. Bush, Interfacial propulsion by directional adhesion, *Int. J. Nonlinear Mech.*, 2011, **46**, 607–615.

10 D. Quere, Fluid coating on a fiber, *Annu. Rev. Fluid Mech.*, 1999, **31**, 347–384.

11 V. Duclaux, C. Clanet and D. Quere, The effects of gravity on the capillary instability in tubes, *J. Fluid Mech.*, 2006, **556**, 217226.

12 F. Vollrath and D. T. Edmonds, Modulation of the mechanical properties of spider silk by coating with water, *Nature*, 1989, **340**, 305307.

13 L. Rayleigh, On the capillary phenomena of jets, *Proc. R. Soc. London*, 1879, **29**, 7197.

14 D. T. Edmonds and F. Vollrath, The contribution of atmospheric water vapour to the formation and efficiency of a spiders capture web, *Proc. R. Soc. London, Ser. B*, 1992, **248**, 145148.

15 B. D. Opell and M. L. Hendricks, Adhesive recruitment by the viscous capture threads of araneoid orb-weaving spiders, *J. Exp. Biol.*, 2007, **210**, 553560.

16 W. Michaeli, *Extrusion Dies for Plastic and Rubber*, Carl Hanser Verlag, Munich, 2003.